

# Determining mean and gradient residual stresses in thin films using micromachined cantilevers

W Fang and J A Wickert

Department of Mechanical Engineering, Carnegie Mellon University, Pittsburgh, PA 15213, USA

Received 9 March 1995, accepted for publication 23 October 1995

**Abstract.** A technique that provides a first approximation to the mean,  $\sigma_0$ , and gradient,  $\sigma_1$ , components of residual stress in a thin-film material is discussed. In this method, measurements are made on a single micromachined cantilever, as opposed to an array of structures as used in the related critical-length buckling approach, to find tensile, compressive and gradient stresses. The measured deflection profile of a cantilever is reduced to rotation and curvature components, which are shown to derive independently from  $\sigma_0$  and  $\sigma_1$ , respectively. Essential to this method is the observation that a micromachined structure with a 'nominally-clamped' boundary undergoes subtle rotation at its junction with the portion of the thin film that remains bonded to the substrate but is contiguous with the structure. This boundary rotation effect occurs through in-plane expansion or contraction of the bonded film following relief of residual stress. Thus, the deformation of the micromachined cantilevers considered here and of more general bulk- or surface-micromachined devices, can be strongly influenced by the state of stress in the still-bonded film.

## 1. Introduction

Characterization and reduction of residual stress in thin-film structures is important in improving the reliability of micro-mechanical, -electronic, -magnetic and -optical devices. With the development of 'micromachining', it is now possible to determine residual stress in a thin film by measuring the elastic deformation of a structure made from it. The advantages of such an approach are two-fold: first, measurements are made on the same dimensional scale as the film of interest and second, because of the intrinsically small size of such structures, the local stress field can be mapped. Thus, the more traditional techniques, in which residual stress is found by measuring the curvature of an entire substrate or wafer, can be supplemented by the use of micromechanical components.

Thin-film structures can deform undesirably as a result of residual stress; on the other hand, these deformations can be exploited to 'diagnose' the state of stress in the film. In the SEM photographs of figure 1, stress gradient through the thickness dimension of the metallic film causes both the surface-micromachined cantilever and gimbal spring to curl. Mean stress can also cause out-of-plane deformation and has been extensively investigated in the context of buckling and post-buckling of fully clamped structures. In general, the state of residual stress in a thin film is complicated, depends on the specifics of the fabrication process and is well known to vary through the film thickness

[1–4]. Stress gradients become particularly acute as the film becomes thinner.

A general uniaxial residual stress field in a thin film can be represented by the polynomial

$$\sigma_{total} = \sum_{k=0}^{\infty} \sigma_k \left( \frac{y}{h/2} \right)^k \quad (1)$$

where  $y \in (-h/2, h/2)$  is the coordinate across the thickness,  $h$ , with an origin chosen at the film's mid-plane. In the first approximation,  $\sigma_{total}$  is the superposition of the constant mean stress  $\sigma_0$  and the gradient stress  $\sigma_1$ , the former being symmetric and the latter anti-symmetric, about the mid-plane. In physical terms, the mean stress can be caused by a mismatch of thermal expansion coefficients between the film and its substrate and the stress gradient by more localized effects including atomic diffusion through  $h$  to the film/substrate interface [5], interstitial or substitutional defects and atomic peening [6].

A variety of approaches have been developed for measuring mean stress using micromechanical components. These techniques involve modelling relationships between the deformation, size and geometry of particular micromachined structures and the stresses acting on them. For instance, the arrays of micromachined clamped-clamped beams of different lengths demonstrated by Guckel *et al* [7] and by Fang and Wickert [8] can be used to determine residual compressive stress, but they remain incapable of

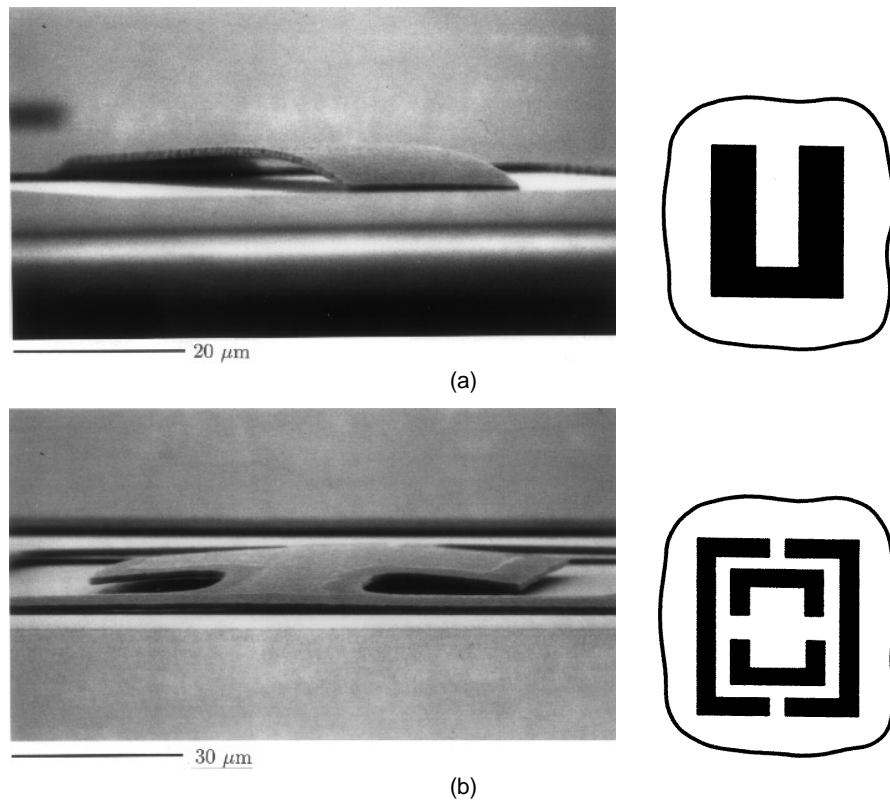


**Figure 1.** SEM photographs of a surface-micromachined titanium showing (a) a cantilever beam and (b) a gimbal spring.

providing estimates for either tensile or gradient stresses. As a result, such buckling-type approaches are restricted to general films and materials in application.

To measure tensile stress, diagnostic structures of greater complexity were designed, including a micromachined ring [9] or ‘T’- and ‘H’-like structures [10]. However, use of even moderately detailed geometries leads to additional model approximations and hence uncertainty in estimates of residual stress. In other approaches, limitations in measurement resolution preclude accurate estimates of tensile stress [1, 10]. In short, compressive stresses can be found from readily modelled and fabricated micromachined beams, whereas tensile stresses have only been found, to date, using more complicated structures.

Quite aside from the issue of mean stress, residual stress fields which have a gradient through the film have been observed in a variety of materials and processes including thermal oxide [1], LPCVD  $\text{Si}_x\text{N}_y$  [2], boron doped  $p^+$  silicon [3, 4], polycrystalline silicon [11, 12] and sputtered titanium as in figure 1. One method of determining gradient stress has been demonstrated by Chu and Mehregany [3] in which the curvature of a micromachined cantilever is measured.

One shortcoming of the available approaches is the ability to measure mean and gradient stresses in a thin film simultaneously and from such a prototypical micromachined structure as the cantilever. In the following text, experiments and a model are discussed which provide tensile/compressive mean stress and gradient stress, by decomposing measured out-of-plane deformations into

components that derive from the mean and gradient stress components independently. The implications of these results for research in the broader area of thin-film micromechanics include the importance of accurately modelling boundary conditions of experimentally realized structures and a re-examination of the ‘clamped’ condition as is commonly applied in the literature.

## 2. Deformation under residual stress

For simplicity, the first two terms in equation (1)—the constant  $\sigma_0$  and linear variation  $\sigma_1$ —are retained in the stress model sketched in figure 2(a), where a thin film in non-uniform residual compression is shown. In this first approximation,  $\sigma_0$  represents the cumulative effect of all symmetric polynomial terms in equation (1) and  $\sigma_1$  represents the influence of the gradient stress anti-symmetric functions. The effect of higher-order terms is thus neglected and

$$\sigma_{\text{total}} \approx \sigma_0 + \sigma_1 \left( \frac{y}{h/2} \right). \quad (2)$$

When a micromachined cantilever is fabricated by removing the film’s supporting substrate, traction at the film–substrate interface is removed, and the structure becomes free to deform out-of-plane following relief of internal stress. As shown in figures 2(b)–(d), the model problem considered here corresponds to deducing, from measured deflections of the cantilever, the uniform and gradient stress components that existed in the original film.

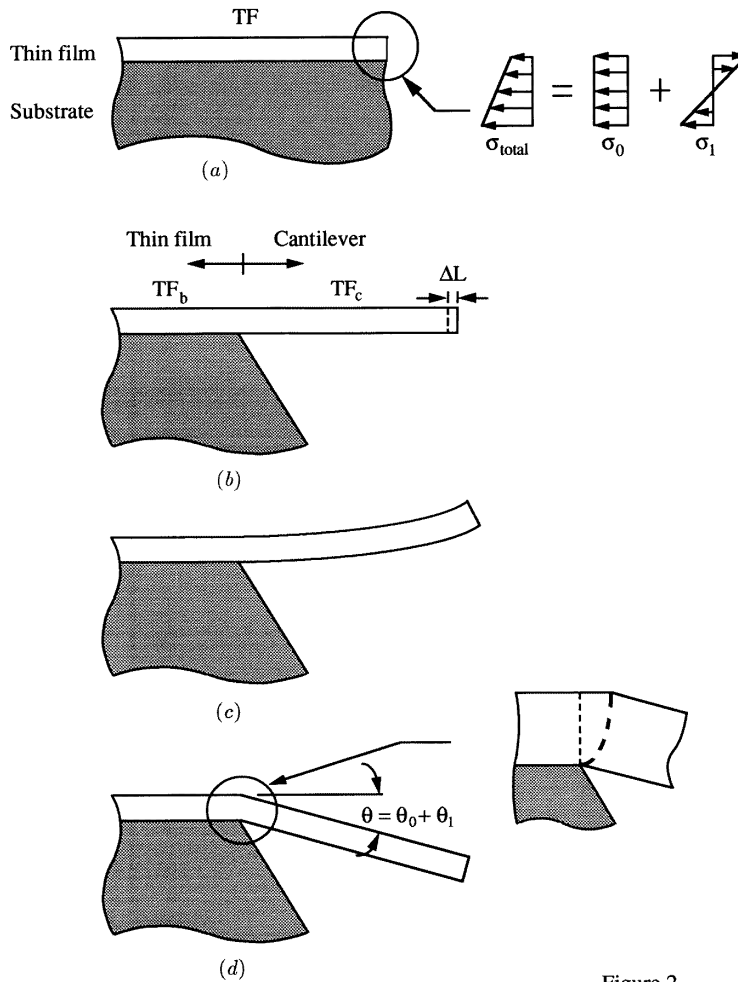


Figure 2

**Figure 2.** States of loading of a thin film. (a) Initial as-deposited or as-grown state, (b) relief from  $\sigma_0$  as the beam changes length, (c) relief from  $\sigma_1$  as the beam undergoes change in curvature and (d) relief from  $\sigma_0$  and  $\sigma_1$  as the boundary rotates.

To model the deformation with accuracy, three states of the film are explicitly identified:

- (i) TF, the original thin film which has not been patterned or etched,
- (ii) TF<sub>c</sub>, the portion of the film that forms the cantilever which deforms after the substrate is removed, and
- (iii) TF<sub>b</sub>, the portion of the film that is bonded to the substrate and remains contiguous with TF<sub>c</sub>.

In short, inclusion of TF<sub>b</sub> and its in-plane deformation in the model is critical in providing the correct boundary conditions to the cantilever, to predict its deformation and to determine  $\sigma_0$  and  $\sigma_1$ .

In figure 2(b), since there is no constraint on the cantilever’s free edge,  $\sigma_0$  is relieved as the beam changes length by  $\Delta L$  [1, 10]. The gradient component,  $\sigma_1$ , on the other hand provides a sensibly constant bending moment to TF<sub>c</sub> and, as a result of such loading, the beam will curl as sketched in figure 2(c). This effect has been used in [3] to find residual gradient stress alone. However, the effect of TF<sub>b</sub> on the deformation of the cantilever has not been considered and yet can play an important role in the mechanics of micromachined structures. The

nominally-clamped end of TF<sub>c</sub> undergoes slight rotation due to an in-plane deformation of TF<sub>b</sub> under relief from the residual stress field. This mechanism is notably distinct from the effects of finite stiffness at ‘step-up supports’ in surface micromachining [13]. As a result, TF<sub>c</sub> is effectively supported by a deformed boundary, as depicted in the inset of figure 2(d), and experiences subtle rotation  $\theta$  as a result of in-plane expansion or contraction of TF<sub>b</sub>. The boundary condition for TF<sub>c</sub> involves zero displacement but a specified slope, which is modelled below as a function of the mean and gradient stresses in the original film TF.

In short, under a general residual stress, TF<sub>c</sub> will deflect out-of-plane, with its far field curvature being generated exclusively by  $\sigma_1$  and with an initial slope determined by both  $\sigma_0$  and  $\sigma_1$ . Characterization of the measured deflections in this manner allows  $\sigma_{total}$  to be estimated.

### 2.1. Modelling

An available finite element package is used to represent the two-dimensional state of stress and deformation of the combined TF<sub>b</sub> and TF<sub>c</sub> structure. In figure 3(a), TF<sub>b</sub> lies in  $(-L_1, 0)$  and is fixed along its entire surface,  $y = -h/2$ , to

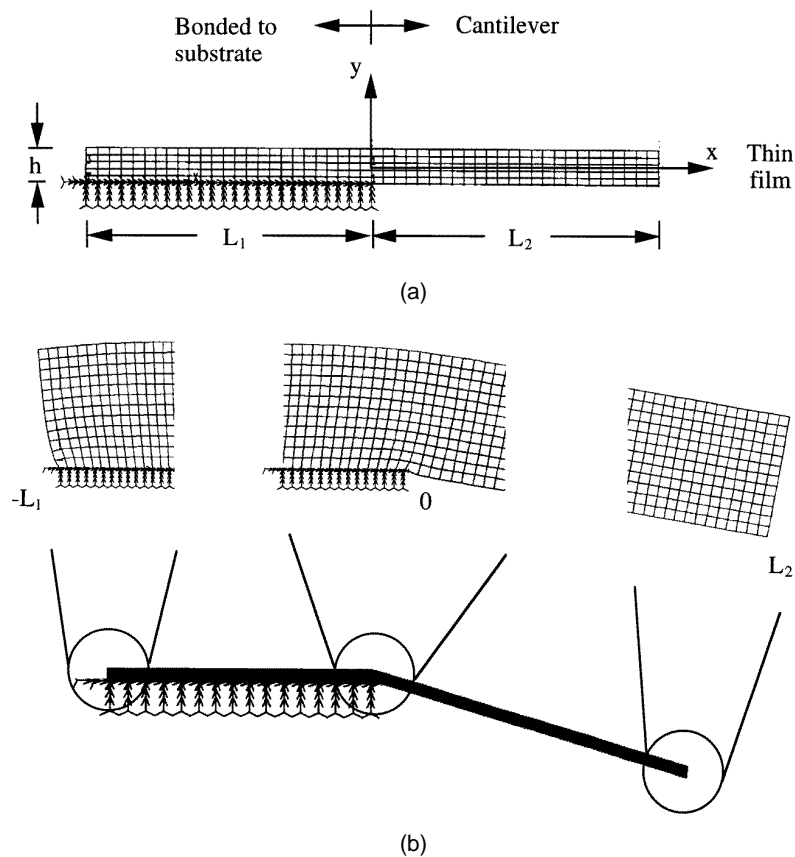


**Figure 3.** (a) Mesh used in the finite element model.  $L_1$  is the length of the bonded film and  $L_2$  is the length of the cantilever. (b) Predicted deformation of the cantilever caused by the relief from mean stress alone. The insets magnify deformations (not to scale) around the discontinuities in geometry.

represent the zero-displacement interface with the substrate. The edge  $x = -L_1$  and upper surface  $y = h/2$  of  $TF_b$  are traction free.  $TF_c$  is located within  $(0, L_2)$  and likewise has a traction free surface except along  $x = 0$  where  $TF_b$  and  $TF_c$  have compatible displacement and stress.

An alternative model, which included elastic deformation of the substrate under  $TF_b$ , was also evaluated. In several test cases, the results from that model and the one discussed above indicated a difference in stresses of roughly 1–3% for silicon substrates with  $SiO_2$  or metallic films. While the thin-film's stresses do depend on the substrate's elastic deformation, for sensible geometries, materials and dimensions relevant to the titled problem, it does not appear to play a significant role in setting the stress values.

Results from the model are shown in figure 3(b), where a silicon dioxide film is considered for illustration; Poisson's ratio  $\nu$  and elastic modulus  $E$  are taken to be 0.17 and 66 GPa, respectively [14]. Predicted deformation of  $TF_b$  and  $TF_c$  when the film is subjected to residual stress  $\sigma_0 = -1.0 \times 10^5$  Pa but  $\sigma_1 = 0$ , is shown in figure 3(b). Portion  $TF_c$  tilts downward (upward) when the film is in residual compression (tension). Deformations in three different regions of the film are of interest. In the left inset of figure 3(b), in-plane distortion of the film is shown near  $x = -L_1$ ; such cross-sectional deformation becomes negligible several film thickness away from either edge,  $x = 0$  or  $-L_1$ , of  $TF_b$ . Similarly, the observed in-plane

deformation near  $x = 0$  propagates several thicknesses into the cantilever. At the free end of  $TF_c$ ,  $x = L_2$ , each element remains rectangular, demonstrating that the cantilever is essentially void of curvature there, although it is tilted relative to the plane of the substrate. In short, the mean stress tends to rotate  $TF_c$  locally near  $x = 0$ , but has little in-plane effect in the far field.

Predicted deformations of a film with  $L_1 = 50 \mu\text{m}$ ,  $L_2 = 50 \mu\text{m}$  and  $h = 2 \mu\text{m}$  required roughly 7200 ( $600 \times 12$ ) elements to converge. Since the  $x/y$  aspect ratio of the elements was held at unity, the element ratio remained  $N_x/N_y = 50$  in convergence studies, as indicated in figure 4(a). This choice of aspect ratio is arbitrary, and is chosen only to simplify illustration of the model's convergence properties; alternative ratios in the range 1/3 to 3 are also acceptable. The convergence characteristics in figure 4(b) show the minimum length  $L_1$  which is required to prevent the interaction of deformations at boundaries  $x = -L_1$  and  $x = 0$  for films of different thicknesses. As a rule of thumb in designing diagnostic structures for residual stress measurement, the influence of the film's in-plane displacement 'propagates' several  $h$  along the beam from such geometric irregularities as those at  $x = -L_1$  and 0. Thus, dimensions  $L_1$  and  $L_2$  should each be greater than about 5–10 film thicknesses to prevent the interaction of boundary effects in neighboring cantilevers formed from the same film. Values of  $L_1 > 50 \mu\text{m}$  were used in all

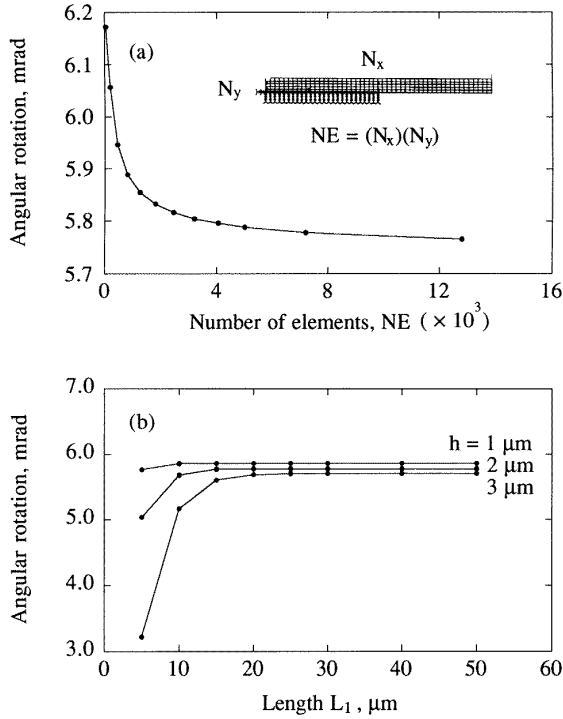


**Figure 4.** Convergence of the model with respect to (a) the number of elements and (b) the length,  $L_1$ , of the film's bonded portion.

subsequent calculations.

## 2.2. 'Tilt' and 'curl' deformations

The total angular rotation of  $TF_c$  is the superposition of components  $\theta_0$  due to mean stress and  $\theta_1$  due to stress gradient and is determined by such variables as residual stress,  $\nu$ , and  $h$ . Parameter studies with the model provided an empirical representation of this relation, and demonstrated that  $\theta_0$  is directly proportional to  $\sigma_0$ , but varies linearly with  $\nu$ . By normalizing  $\theta_0$  with respect to those factors, the scaled angle  $\theta_0^* = \theta_0(E/\sigma_0)/(1.33 + 0.45\nu)$  is defined. In figure 5a, the model's dependence of  $\theta_0^*$  on  $h$  is linear, and so

$$\theta_0 \approx \frac{\sigma_0}{E}(1.33 + 0.45\nu)(-0.014h + 1.022) \quad (3)$$

where  $h$  has units of  $\mu\text{m}$ . Thus, with  $\nu$ ,  $E$  and  $h$  being known, the residual stress component  $\sigma_0$  can be obtained from equation (3) when the tilt angle  $\theta_0$  is measured and, importantly, when TF is known to be void of gradient stress.

Since gradient stress is present in the general case, its contribution  $\theta_1$  to rotation at the base of the cantilever is also characterized. Based on an analogous empirical fit,

$$\theta_1 \approx \frac{\sigma_1}{E}(0.0086h^2 - 0.047h + 0.81) \quad (4)$$

as shown in figure 5(b). Relations (3) and (4) have been evaluated over  $0.1 \leq \nu \leq 0.4$ ,  $0.5 \mu\text{m} \leq h \leq 3.0 \mu\text{m}$ ,  $10^{-4} < \sigma_0/E < 10^{-1}$  and  $10^{-4} < \sigma_1/E < 10^{-1}$  and appear to well represent  $\theta_0$  and  $\theta_1$  within those parameter ranges.

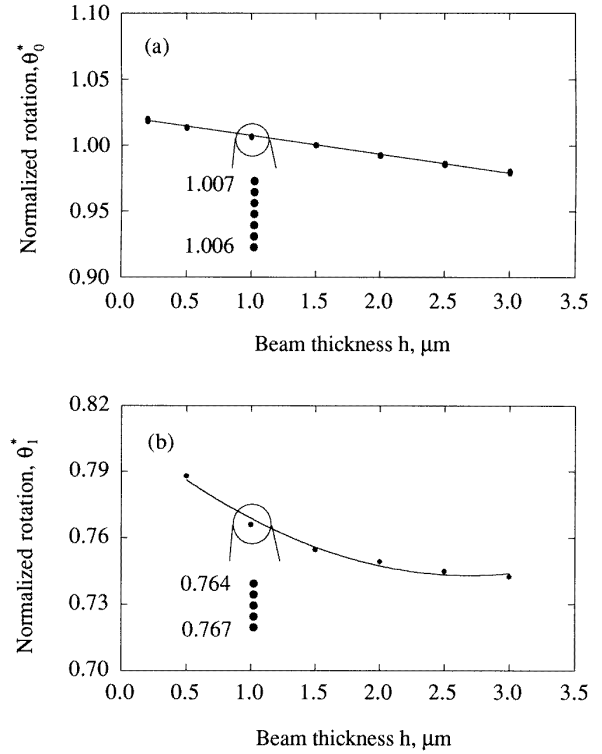


**Figure 5.** Predicted base rotation of a cantilever in the presence of (a) mean and (b) gradient stresses. The solid lines are obtained by a curve fit of the model results shown for  $\nu = 0.1, 0.15, \dots, 0.4$  and are given by equations (3) and (4).

In addition to base rotation, gradient stress also causes out-of-plane deflection with a constant radius of curvature,  $R$ , [15] and the peak value,  $\sigma_1 = Eh/2R$ , of the gradient stress can therefore be found by measuring the curvature of  $TF_c$ .

The net deflection of  $TF_c$  is found by superposing the effects of  $\sigma_0$  and  $\sigma_1$ . Since the residual strain is typically less than 0.1%,  $L_2$  is taken as constant. The transverse deflection becomes

$$y \approx (\theta_0 + \theta_1)x + \frac{1}{2R}x^2 \quad (5)$$

for  $x \in (0, L_2)$ . Four permutations of the cantilever's profile are possible, as shown in figure 6, where results from the model with the illustrative values  $\sigma_0 = \pm 1.0 \text{ kPa}$  and  $\sigma_1 = \pm 0.9 \text{ kPa}$  in  $\text{SiO}_2$  are shown. With compressive mean stress and a negative gradient, for instance, experimentally characterized cantilevers are expected to have negative slope at the base of the cantilever and negative curvature along its length. Conversely, when  $\sigma_0$  changes sign, representing residual tension, the slope at the  $TF_b$ - $TF_c$  junction becomes positive. In this manner, the tensile and compressive mean stress as well as the gradient stress can be obtained by decomposing the measured deflection profile of  $TF_c$  into its constituent linear and quadratic components in accordance with equation (5).

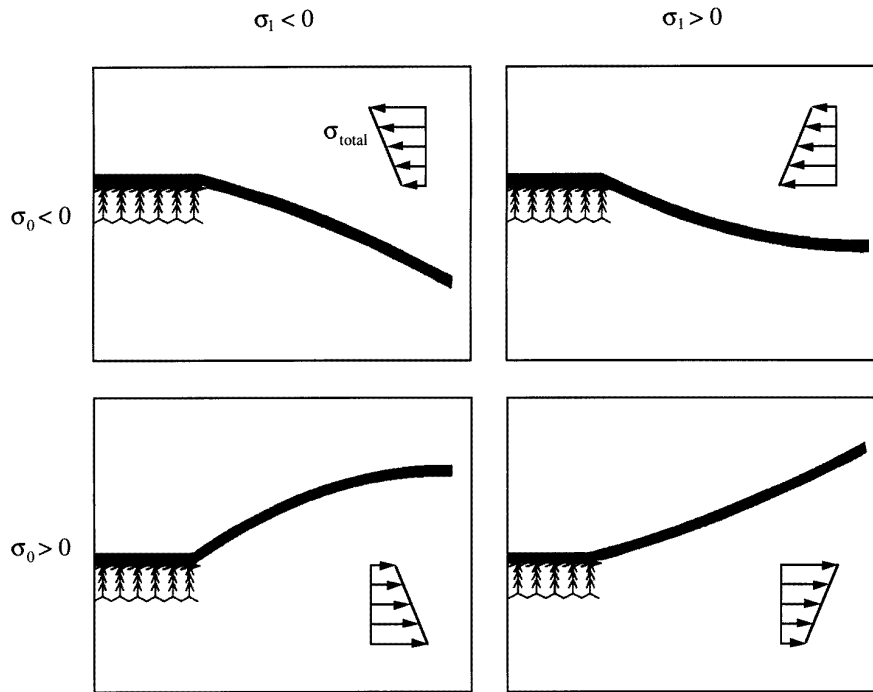


**Figure 6.** Four possible profiles of micromachined cantilevers following relief from general mean and gradient stresses, as predicted by the model.

### 3. Application and results

In application of this technique,  $\text{SiO}_2$  beams with lengths between 50 and 150  $\mu\text{m}$  were fabricated through bulk micromachining. Cantilevers of different lengths were examined to check the consistency of the measurements but, unlike methods for measuring mean compressive stress through critical-length buckling of beams [7–9], use of a beam array is not necessary in the present technique. An  $\text{SiO}_2$  layer was thermally grown at 1100  $^\circ\text{C}$  on a polished single-crystal silicon substrate with (100) orientation. The substrate was etched anisotropically with a 33–38% KOH solution at 85  $^\circ\text{C}$  and, when relieved from the substrate, the completed oxide beams (namely,  $\text{TF}_c$ ) were suspended above a pyramidal cavity with {111} sidewalls. Because the substrate was several hundred times thicker than the film and since the dimension  $L_1 \approx 200 \mu\text{m} \gg h$ , neighboring beams were assumed to be uncoupled in their deflections.

Profiles of the cantilevers were measured through white light interferometric profilometry. The fringe pattern generated by interference between light reflected from a reference surface and from a target microbeam provided the three-dimensional profile. The fringes, in turn, were digitized by a 256 $\times$ 256 element CCD camera using a commercial ‘Wyko-3D’ system. In the present case, the imaged field of view with a 40 $\times$  objective lens was approximately 250  $\mu\text{m}$  by 250  $\mu\text{m}$ . Typical measured profiles of four 1  $\mu\text{m}$  thick, 20  $\mu\text{m}$  wide beams with lengths from 100 to 150  $\mu\text{m}$  are shown in figure 7(a). The profile of the 100  $\mu\text{m}$  beam is shown in figure 7(b) as a section along the  $x$ -axis, in which rotation at the base of the cantilever is evident.

In figure 8, the measured profile for a cantilever of 2  $\mu\text{m}$  thickness is broken down into its linear ‘tilt’ and quadratic ‘curl’ components. The flow chart outlines this decomposition into initial slope and curvature. The unknown coefficients  $\theta_0 + \theta_1$  and  $1/2R$  in equation (5) are obtained by a least squares fit of the measured deflection to the model. In the case of the 120  $\mu\text{m}$  cantilever depicted in figure 8, the best fit is obtained with  $\theta = -6.10$  mrad and  $1/2R = 42 \text{ m}^{-1}$ . With this value of  $R$ , the peak gradient stress becomes  $\sigma_1 = 1.350$  MPa and the rotation that arises from  $\sigma_1$  alone is calculated from equation (4) as being  $\theta_1 = 0.015$  mrad. Since  $\theta$  is evidently some two orders of magnitude greater than  $\theta_1$ , rotation of the cantilever is caused primarily by the residual mean stress, which is calculated in equation (3) as  $\sigma_0 = -0.286$  GPa. Thus, the first approximation to the total residual stress field specifies a variation from a value of  $\sigma_{\text{total}} = -0.285$  GPa at the free surface  $y = h/2$ , to  $\sigma_{\text{total}} = -0.287$  GPa at the interface between the film and substrate. This stress distribution is consistent with that of a previous investigation [16]. In figure 9, the measured profile is compared to that predicted by the finite element model in which the present values of  $\sigma_0$  and  $\sigma_1$  are used. Over the length of the cantilever, the root mean square error for pointwise prediction of deflection is 0.0044  $\mu\text{m}$ , some 1% of the tip deflection.

A similar flow chart for a 1  $\mu\text{m}$  thick cantilever is shown in figure 10, and in this case the residual stress components become  $\sigma_0 = -0.276$  GPa and  $\sigma_1 = 2.180$  MPa. These 1 and 2  $\mu\text{m}$  films were grown simultaneously, with the only difference being in the furnace exposure time. Because of the fabrication process, the residual stress of thermally-grown oxide is dominated by the difference

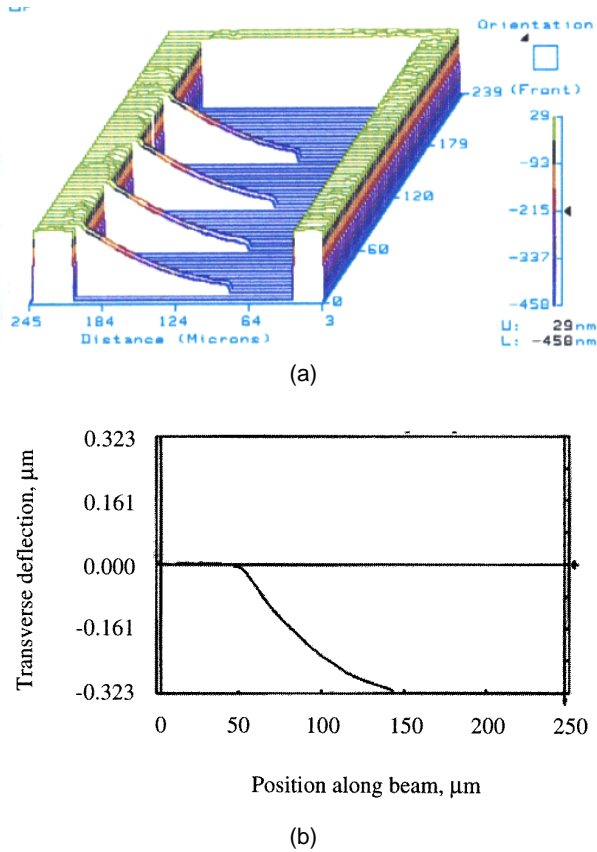


**Figure 7.** Measured deflections from interferometric profilometry. (a) A three-dimensional profile of beams with  $100 \mu\text{m} \leq L \leq 150 \mu\text{m}$  and (b) an  $x$ -axis profile of the  $100 \mu\text{m}$  beam.

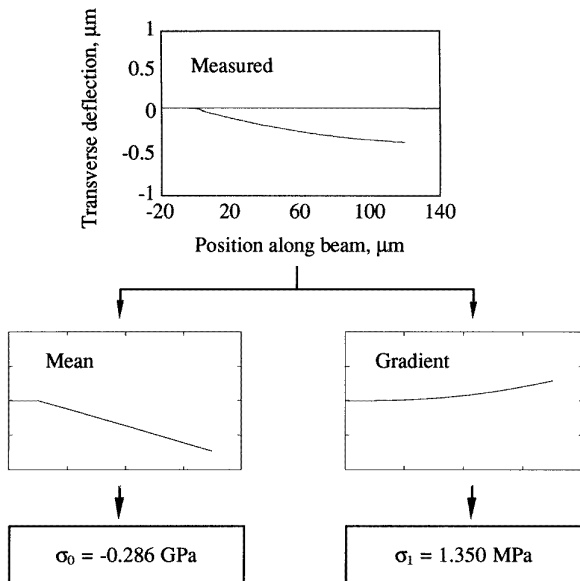


**Figure 8.** The measured profile of a  $2 \mu\text{m}$  thick beam, which is decomposed into linear and quadratic components that derive essentially from  $\sigma_0$  and  $\sigma_1$ .

of thermal expansion coefficients,  $\Delta\alpha$ , between the film and substrate, and the difference in temperatures,  $\Delta T$ ,

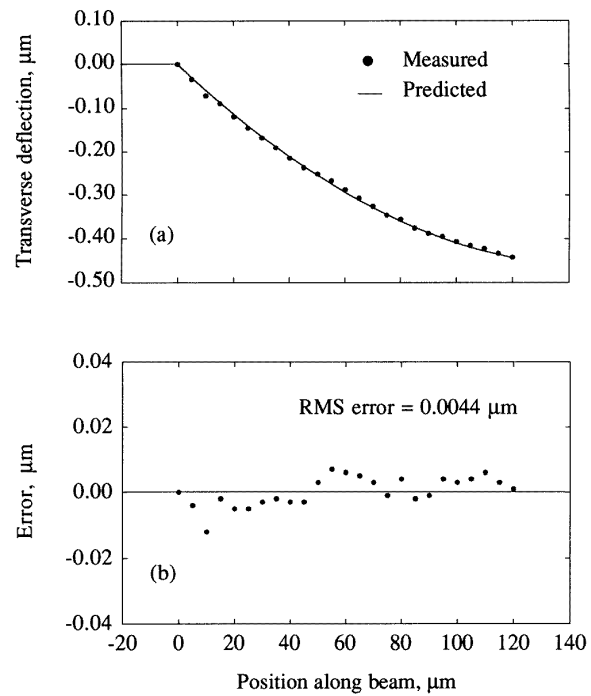


**Figure 9.** (a) A comparison of the measured and predicted profiles of a  $2 \mu\text{m}$  thick beam and (b) the pointwise distribution of error.

between the room and furnace. Since  $\Delta\alpha\Delta T$  of the two films are nearly equal, the mean stresses measured in the two cases are essentially the same, differing by only some 3%.  $\text{SiO}_2$  samples investigated previously [8] were prepared identically to those used in this study and  $\sigma_0$  values measured through these two different techniques agree to within 3–6%. The gradient stress on the other hand, arises primarily from oxygen diffusion while the film is forming [5] and thus differs by roughly 50% between the two films because of differing durations at elevated temperatures. Despite the relative difference between magnitudes of the  $\sigma_0$  and  $\sigma_1$  values, inclusion of each in the model is important because under their combined effect the micromachined cantilever can have a positive tip deflection in one case and a negative deflection in the other, as evidenced in figures 8 and 10.

#### 4. Summary

To predict the deformation of micromachined structures, it is important to accurately treat their boundary conditions. Strictly speaking, even for the simplest cantilever structures such as those discussed here, the boundary is not ‘clamped’ in the sense of having zero initial slope and this phenomenon can be exploited to find the residual stress. One feature of this technique is that the residual mean (tensile or compressive) and gradient stresses can be determined simultaneously by the measurement of a single cantilever.

Accurate measurement of the thickness of a micromachined structure is difficult once the substrate or sacrificial

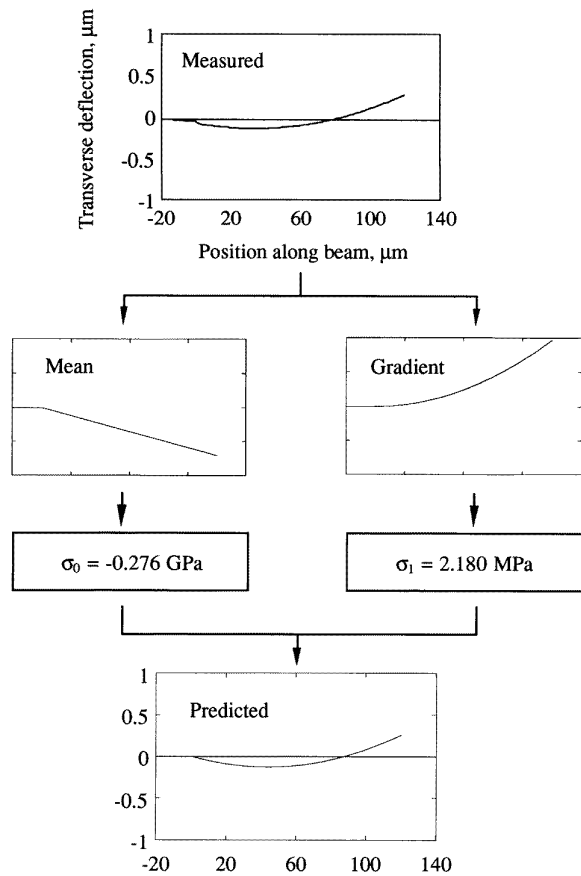


**Figure 10.** A comparison of the measured and predicted profiles of a 1  $\mu\text{m}$  thick beam and the decomposition into the  $\sigma_0$  and  $\sigma_1$  components. The RMS error of the predicted pointwise deflection is 0.0048  $\mu\text{m}$ .

supporting layer has been removed. The present technique provides an estimate of  $\sigma_0$  in which the propagation of measurement error in  $h$  is reduced. In critical-length buckling techniques [7], the relative error in  $\sigma_0$  is twice that of the measured film thickness, as given by  $d\sigma_0/\sigma_0 = -2dh/h$ . However, error propagation in equation (3) satisfies

$$\frac{d\sigma_0}{\sigma_0} = \frac{0.014dh}{(-0.014h + 1.022)} \quad (6)$$

For instance, the error in  $\sigma_0$  for a 1  $\mu\text{m}$  thick film with a  $dh/h = 10\%$  is reduced to just 0.14% rather than the 20% realized in the buckling approach.

Accounting for boundary rotation, and the calibration of models to correct for it, can be useful in improving related residual stress techniques. One such approach involves depositing a thin film of interest on a cantilever beam and obtaining the residual stress by measurement of its deflection [17]. The radius of curvature for the so-called bi-material beam is frequently determined in practice through the relation  $R \approx L^2/2\delta$ , where  $\delta$  is the cantilever's tip deflection. However, because of the potential initial slope of the cantilever in the light of Eqs. (3)-(4), this tip deflection method should be restricted in application to films in which rotations are known *a priori* to be negligible.

Interestingly, tip deflection can be highly sensitive to the stress state, even when beams are made of the same material, to the degree that tip deflections of opposite sign are observed (see figures 8 and 10).

One application of the results beyond microcantilevers can be found in the buckling of fully clamped microstructures. Buckling and post-buckling techniques require knowledge of the imperfection level, representing non-ideal loading, fabrication defects and geometric irregularities of the beam [1, 7]. The angular deflection,  $\theta$ , and the gradient residual stress,  $\sigma_1$ , discussed here are two candidate sources of such imperfection. Other potential applications of the boundary rotation phenomenon include elastic constant measurement [18], capillary force studies [19] and micromachined sensors [20].

## Acknowledgments

This material is based (in part) upon work supported by the National Science Foundation under Grant ECD-8907068.

## References

- [1] Lin S C H and Pugacz-Muraszkiewicz I 1972 Local stress measurement in thin thermal  $\text{SiO}_2$  films on Si substrates *J. Appl. Phys.* **43** 119-125
- [2] Kiesewetter L, Zhang J-M, Houdeau D and Steckenborn A 1992 Determination of Young's moduli of micromechanical thin films using the resonance method *Sensors and Actuators A* **35** 153-159
- [3] Chu W-H and Mehregany M 1993 A study of residual stress distribution through the thickness of  $p^+$  silicon films *IEEE Trans. on Electron Devices*. **40** 1245-1250
- [4] Ding X, Ko W H and Mansour J M 1990 Residual stress and mechanical properties of boron-doped  $p^+$ -silicon films *Sensors and Actuators* **21-23** 866-71
- [5] Campbell J D S 1970 Mechanical properties of thin films *Handbook of Thin Film Technology* eds L I Maissel and R Glang (New York: McGraw-Hill)
- [6] Thornton J A and Hoffman D W 1989 Stress-related effects in thin film *Thin Solid Films* **171** 5-31
- [7] Guckel H, Randazzo T and Burns D W 1985 A simple technique for the determination of mechanical strain in thin films with application to polysilicon *J. Appl. Phys.* **57** 1671-75
- [8] Fang W and Wickert J A 1994 Post-buckling of micromachined beams *J. Micromech. Microeng.* **4** 116-22
- [9] Guckel H, Burns D, Rutigliano C, Lovell E and Choi B 1992 Diagnostic microstructures for the measurement of intrinsic strain in thin films *J. Micromech. Microeng.* **2** 86-95
- [10] Mehregany M, Howe R T and Senturia S D 1987 Novel microstructures for the in situ measurement of mechanical properties of thin films *J. Appl. Phys.* **62** 3579-84
- [11] Burns D W and Guckel H 1990 Thin films for micromechanical sensors *J. of Vac. Sci. Technol. A* **8** 3606-13
- [12] Howe R T and Muller R S 1983 Polycrystalline silicon micromechanical beams *J. Electrochem. Soc.* **130** 1420-3
- [13] Meng Q, Mehregany M and Mullen R L 1993 Theoretical modeling of microfabricated beams with elastically restrained supports *J. Microelectromechanical System* **2** 128-37

- [14] Runyan W R and Bean K E 1990 *Semiconductor Integrated Circuit Processing Technology* (Reading, MA: Addison-Wesley)
- [15] Timoshenko S and Woinowsky-Krieger S 1959 *Theory of Plates and Shells* (New York: McGraw-Hill)
- [16] Kobeda E and Irene E A 1988  $SiO_2$  film stress distribution during thermal oxidation of Si *J. of Vac. Sci. Technol. B* **6** 574-8
- [17] Johansson S, Ericson F and Schweitz J 1989 Influence of surface coatings on elasticity, residual stresses, and fracture properties of silicon microelements *J. of Appl. Phys.* **65** 122-8
- [18] Petersen K E and Guarnieri C R 1979 Youngs modulus measurements of this films using micromechanics *Journal of Applied Physics* **50** 6761-5
- [19] Mastrangelo C H and Hsu C H 1993 Mechanical stability and adhesion of microstructures under capillary forces, I. Basic theory *J. Microelectromechanical System* **2** 33-43
- [20] Fatah R M A 1992 Mechanisms of optical activation of micromechanical resonators *Sensors and Actuators A* **33** 229-36